Experimental observation of thermoplasmonic heat transfer at the nanoscale by polymerization.
A step towards nanoscale heat sources.

Amine Khitous[1,2], Céline Molinaro[1,2*], Stephania Abdallah[1,2], Jean-Pierre Malval[1,2], Sylvie Marguet[3], Olivier Soppera[1,2*]

[1] *Université de Haute Alsace, CNRS, IS2M UMR 7361, F-68100 Mulhouse, France*

[2] *Université de Strasbourg, France*

[3] *Université Paris-Saclay, CEA, CNRS, NIMBE, F-91191 Gif-sur-Yvette, France*

Contact: céline.molinaro@uha.fr; olivier.soppera@uha.fr

Abstract

The thermoplasmonic effect, arising from the relaxation of a metal nanostructure excited at plasmon resonance, has garnered significant interest in recent years. While this effect has been extensively studied across various spatial and temporal scales, there is currently no experimental technique for investigating the spatial distribution of heat exchange at the nanoscale. In this paper, we introduce a chemical approach to map the temperature distribution around nanoparticles. Formulations that crosslink at specific temperatures are placed in contact with gold nanotriangles and irradiated under controlled power and polarization conditions. At moderate power, the polymerized regions, corresponding to the zones of maximum field, exhibit local temperatures exceeding the polymerization temperature. At higher power, anisotropic melting of the gold within the gold nanotriangles was observed. This new methodology reveals that, contrary to common assumptions, significant heat exchange occurs between the nanoparticle and the surrounding medium before temperature homogenization within the nanoparticle. We have thus demonstrated the potential to generate nanoscale heat sources, representing a major advance on a fundamental level and opening up numerous new prospects in nanofabrication.

Keywords: localized surface plasmon resonance (LSPR), thermoplasmonics, nanostructuring, polymerization, nanoparticles.

Introduction

The thermoplasmonic effect is defined as the thermal effect generated by the excitation of metallic nanostructures under plasmonic resonance conditions. This phenomenon corresponds to one of the deactivation processes following photon absorption by a metallic nanostructure at

plasmonic resonance. In recent years, there has been considerable interest in this effect, due to its applications in fields as diverse as medecine[1,2], catalysis[3,4], energy[5], water treatment[6], photonics[7–9] and thermoelectric devices[10–12]. This interest stems in particular from the high conversion efficiency of light energy into heat, which can reach 80%[13,14] and the ability to easily modulate the absorption spectrum of nanostructures by choosing the material, shape and/or size of the nanostructures.

A large number of studies have focused on investigating this effect in recent years, proposing experimental or numerical approaches applicable to different scales[15–19]. Determining and optimizing the temperature achieved through thermoplasmonics is a major challenge for the development of practical applications. This involves not only determining the temperature reached and the dynamics of the phenomena involved, but also understanding how this temperature can be effectively transferred to the surrounding medium.

When nanoparticles are present at high surface or volume densities, the heating effect is collective and observable on a macroscopic scale. It can then be quantified by conventional temperature measurement techniques using a thermocouple or thermal camera[20–24].

For nanoparticles that are distant enough to reduce collective effects, most of the methods developed are based on optical methods such as fluorescence. [25], Raman spectroscopy[26] or optical imaging[16]. Although these methods offer very high sensitivity and accuracy in terms of temperature, their spatial resolution is limited by diffraction. They can therefore be used to quantify these effects on scales of a few hundred nm, i.e. much larger than the nanostructures that generate the effect.

From a temporal point of view, transient spectroscopy methods show that after plasmon excitation (10 fs), radiative de-excitation processes are very rapid, on the order of 100 fs for electron-electron interaction and 1-10 ps for electron-phonon interaction[27]. Relaxation by phonon-phonon interaction occurs on the scale of tens of ns[28,29]. In terms of heat transfer with the external environment, it is assumed that the temperature inside the nanoparticle is homogeneous. However, recent work has focused on describing the spatial distribution of temperature within the nanoparticle and its temporal evolution.

Numerical approaches have also been developed to describe the phenomenon at the nanoparticle scale[14,19,30–32] from a spatio-temporal point of view. Recent studies include the work of Bryche et al[29], who show computationally that electronic and lattice temperatures are anisotropically distributed over time scales of a few hundred fs before homogenizing at the surface of nanostructures.

However, experimental approaches have demonstrated non-homogeneous thermal phenomena in nanoparticles, leading to local nanoparticle fusion, for example. For example, Viarbitskaya et al recently demonstrated the anisotropic fusion of submicrometer particles according to the polarization of light[17]. More recently, Zhang et al have demonstrated that the excitation of metal nanostructures by a linearly polarized pulsed laser enables the anisotropic melting of aluminum crosses, according to the arm parallel to the polarization of the incident light. This concept has been applied to the preparation of metasurfaces[15]. These examples therefore demonstrate the possibility of generating non-homogenous thermal phenomena at the nanoparticle scale. However, in these examples, the focus is on effects inside the nanoparticle, which does not correspond to the effects sought in applications where heat must be transmitted to the outside environment. It is also important to note that these approaches are based on the assumption that macroscopic physical constants are used to describe nanomaterials, which can lead to significant discrepancies in the results obtained, such as the thermal conductivity[33–35] and melting temperature of metallic nanomaterials[36]. For example, several studies have shown that the thermal conductivity of nanomaterials decreases significantly due to increased electron scattering at the nanoparticle surface[33–35].

To date, there is no experimental method to map local heat transfer on a scale smaller than that of a nanoparticle.

Here, we propose a new method based on chemical mapping using a thermal polymerization reaction. This method is derived from work on near-field photopolymerization, which has proved very useful for mapping the optical near-field using a material that can be photopolymerized at the nanoparticle excitation wavelength.[37–41]. To address the thermoplasmonic issue, we propose in this work to use a thermopolymerizable resin instead of a photopolymerizable resin. This resin, developed by C. Molinaro, has proved its worth for characterizing thermoplasmonic effects on a macroscopic scale in the context of collective effects.[42]

This acrylate-based thermoresponsive resin is used to study for the first time the heat transfer between a nanoparticle and the surrounding dielectric medium. Analysis of nanoparticles by transmission electron microscopy (TEM) enables spatial resolution down to the nanometer scale. It is then possible to study heat exchange at the nanometric scale, under different power and polarization states of the exciting light. In this study, we are interested in gold nanotriangles, but the methodology can be extended to any type of colloidal nanoparticle. In addition to advancing our understanding of this fundamental phenomenon, this new approach opens up the possibility of applications involving a nanoscale heat source, particularly for nanofabrication.

Experimental section

Synthesis and deposition of Au nanotriangles (AuNTs) : Gold nanoplates (dimension: 73 ± 3 nm, Rc: 9 ± 1 nm × thickness: 15 nm) were synthesized by colloidal route in aqueous solution[43]. They are deposited in low concentration on a TEM grid (this grid consists of two rectangular windows (1500 µm × 100 µm) covered with a 50 nm-thick Si3N4 membrane supplied by Ted Pella Inc) to avoid coupling between nanoparticles and thus enable a study of individual nano-objects. To remove the surfactant stabilizing the AuNTs, 200 µl of the AuNTs solution was diluted in 800 µl of pure water and centrifuged (3500 g for 15 min). After deposition, the TEM grid was exposed to UV-ozone treatment for 2 hours, then gently rinsed with deionized water and ethanol (see our recent work for more details[44]). TEM images of post-treatment AuNTs confirm the effective removal of surfactant (CTAB) from around the AuNTs.

Thermopolymerizable resin: The formulation used in this study includes a dialkoxyamine radical polymerization initiator (DIAMS)[45,46] and a triacrylate monomer Pentaerythritol triacrylate (PETA, Sigma Aldrich). The trifunctional monomer used in free-radical polymerization ensures very high cross-linking rates at low conversions, enabling nanometric resolutions to be achieved, as shown below. The formulation noted F_{DIAMS} contains 3 wt % DIAMS. This composition enables polymerization at a temperature of 143°C (**Figure 1.b**). In addition, the monomer without thermal initiator was also tested for comparison. Thermal self-polymerization of PETA was observed at 216°C (**Figure 1.b**). Optical properties of the formulations were characterized by UV-visible spectroscopy (PerkinElmer Lambda 35 UV/VIS) and thermal properties by differential scanning calorimetry (Mettler-Toledo DSC1).

Irradiations: After deposition of the AuNPs on the TEM grid, a drop of F_{DIAMS} is deposited on the TEM grid, which is then mounted on a 3D piezoelectric stage, enabling the sample to be moved under the focused beam, via Zeiss Axio Observer D1 inverted microscope. Excitation takes place at a wavelength of 800 nm, with a Ti:Sapphire mode-locked oscillator (Coherent, Chameleon Ultra II) offering a pulse duration of 140 fs and a repetition rate of 80 MHz. The intensity of the incoming laser is adjusted using an acousto-optic modulator. The laser used is linearly polarized with a known polarization direction at the sample surface. The incident beam is focused through a 0.95 NA (×40) objective, producing a radial spot size of 450 nm. The sample travel speed is 10 µm/s. After irradiating the AuNTs covered by F_{DIAMS}, the TEM grid

is rinsed with acetone and ethanol to remove unreacted formulation. The samples are then observed by TEM (high-resolution transmission electron microscope JEOL ARM200F).

Simulations : The absorption, scattering and extinction cross sections and field maps were obtained by numerical simulations carried out using the MATLAB toolbox Metallic Nanoparticles Boundary Element Method(MNPBEM).[47,48] Nanotriangle dimensions were deduced from TEM and AFM measurements (dimension: 73 nm, Rc: 9 nm × thickness: 15 nm). The simulations were performed s in an environment as closed as the one used in the irradiation step. A single AuNT was considered in a medium of a refractive index RI_{FDIAMS} = 1.48 (index of the formulation). This particle is located at 1 nm above the substrate (corresponding to the thickness of the residual surfactant under the NT, RI_{CTAB} = 1.48). The substrate (RI_{SI3N4} = 2.02)[49] is considered infinite. The refractive index of Au is taken from Johnson and Christy[50].

The Au NT is illuminated through the substrate under normal incidence with linear polarization (in-plane angle adjustable). All simulations are performed in retarded mode. The fields maps have been carried out with illumination at an 800 nm wavelength. All maps show the squared modulus of the electric field in top view through the equatorial plane of the AuNT.

Results and discussion

The aim here is to use thermopolymerizable resin to investigate nanoscale heat generation from nanoparticles. The composition and properties of the resin, already validated on a macroscopic scale, are shown in **Figure 1**.

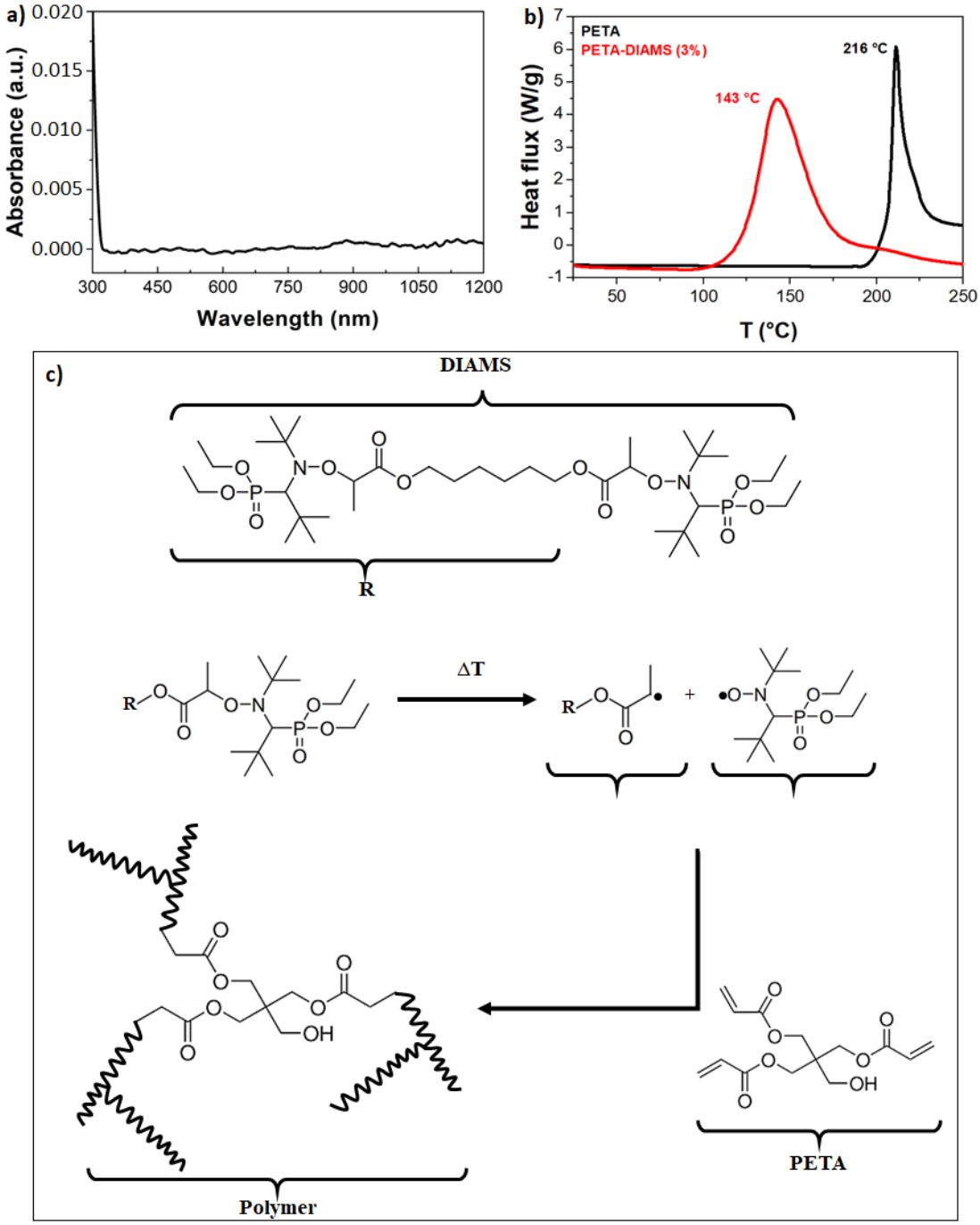

Figure 1 : a) UV-visible spectrum of F_{DIAMS}, **b)** Heat flux analysis for F_{DIAMS} and PETA; **c)** Schematic of the mechanism for thermal decomposition of DIAMS mechanism of DIAMS and PETA polymerization.

This resin is composed of a triacrylate monomer and a thermal initiator the decomposition temperature of which can be determined by DSC at 143°C as shown in **Figure 1b**. This figure also shows the thermal properties of the monomer alone (PETA). Its self-polymerization temperature is reached at 216°C. This difference clearly shows that the thermal polymerization process is initiated by the decomposition of the initiator, as schematically illustrated in **Figure**

1c. The accepted mechanism for these initiators is homolytic breakdown, producing free-radical species that enable the polymerization of acrylic monomers. Note that the choice of a solvent-free trifunctional monomer offers a very high concentration of polymerizable C=C double bonds. These conditions are favorable for radical polymerization, resulting in a highly cross-linked system at low conversion rates (**Figure 1d**). The choice of radical chemistry is also justified by its sensitivity to oxygen. Carbon radicals react with oxygen to create peroxide radicals that are non-reactive for polymerization[40]. This pathway therefore corresponds to a polymerization termination pathway. It is responsible for an induction period, but also plays a crucial role in nanofabrication by confining the spatial extension of the radical reaction[40]. These conditions are important for achieving nanoscale resolution, as shown in photochemical approaches[37,39,51,52]. **Figure 1.a** shows the absorption spectrum of the formulation. Note the absence of absorption above 320 nm, thus excluding purely photochemical excitation with a 800 nm illumination. This property was verified by irradiation experiments in which the formulation placed on a microscope coverslip was irradiated with a power of 1200 mW, much higher than the powers typically used in the presence of NPs (of the order of 30-100 mW). These conditions are higher than the power densities that can be envisaged in the near-field[53,54]. Under these conditions, no polymerization was observed, allowing us to exclude any reaction directly photoinduced by mono- or multiphoton absorption.

This formulation is deposited on the nanoparticles and the system is irradiated at 800nm in pulsed mode. The nanoparticles chosen are nanotriangles. Their dimensions enable them to excite plasmonic resonance at 800 nm (**Figure 2.a**). Depending on the polarization direction, two different modes can be excited, as shown on the field maps (**Figure 2b**). Note that the extinction spectra are similar for both polarization directions.

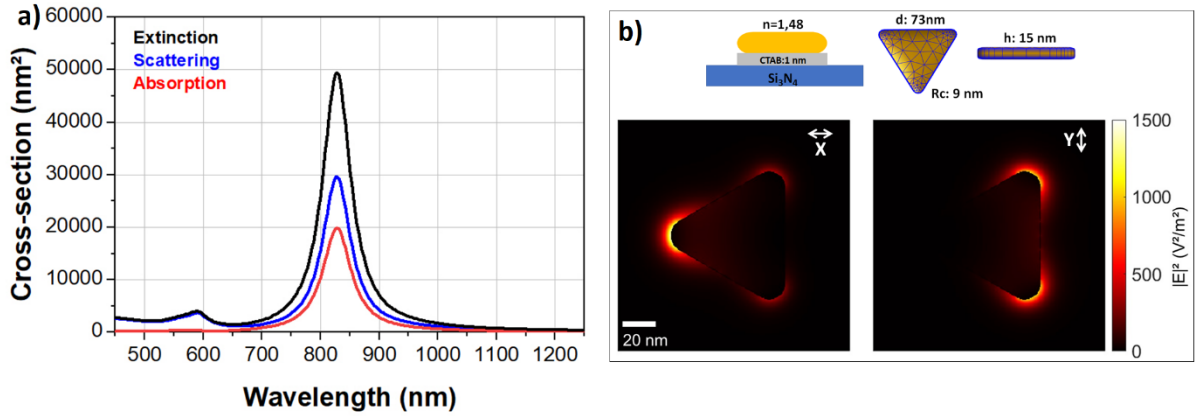

Figure 2: a) Extinction, absorption, and scattering spectra of AuNTs in the configuration shown above, depending on the X and Y polarization of the light. **b**) Field maps of AuNTs based on the light polarization, X and Y, in the configuration shown on the left.

After irradiation with different incident powers and rinsing to remove non-crosslinked polymer, the samples are observed by TEM. Typical images for a given orientation of the nanotriangles with respect to the polarization direction are shown in **Figure 3**.

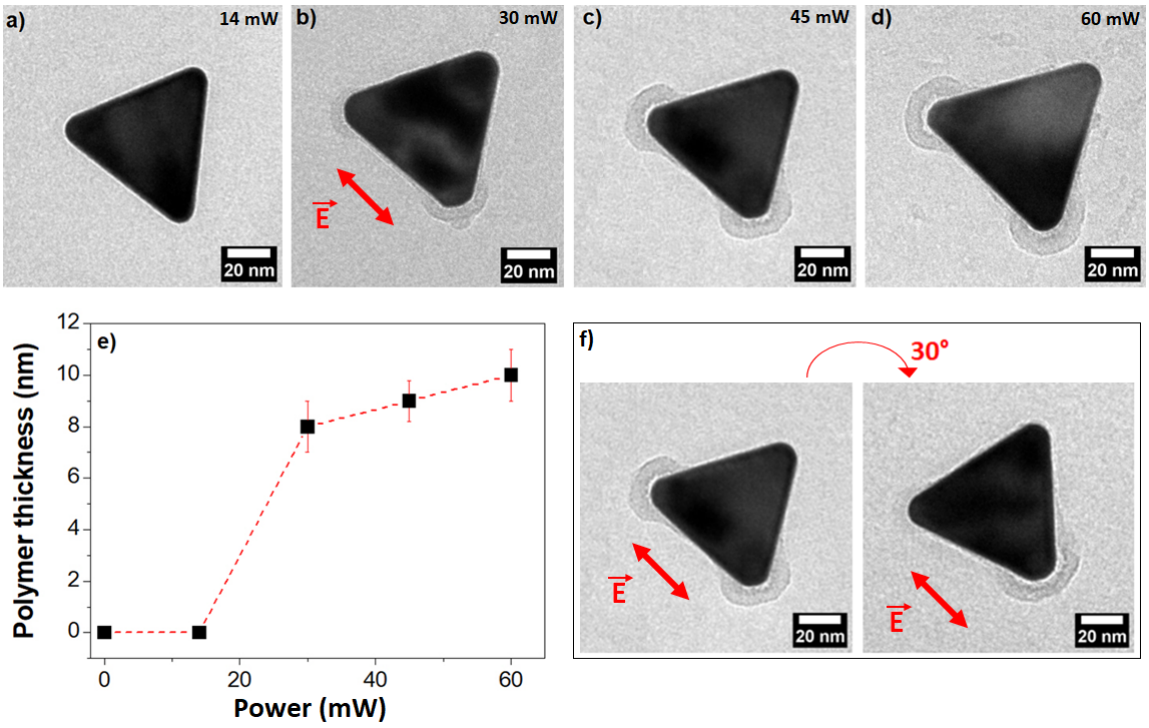

Figure 3. TEM images of AuNPs after irradiation in F_{DIAMS} at different powers: **a**) 14 mW, **b**) 30 mW, **c**) 45 mW, **d**) 60 mW. **e**) Effect of power on the size of polymer lobes. **f**) Effect of polarization direction on polymerization of F_{DIAMS} at 60 mW (direction of polarization is given by the red arrow).

At powers below 14 mW, no traces of polymer were observed. Moreover, this result shows that the NPs washing procedure effectively removes the surfactant. The procedure for removing unreacted resin is also effective.

At 30 mW, two polymer lobes appear. Remarkably, these polymer lobes are located at both ends along the edge parallel to the light polarization indicated by the red arrow. These polymer lobes therefore appear in the zone of maximum field while compared with the field maps shown previously.

Results obtained on other particles irradiated with 45 mW and 60 mW confirm these results, with the volume of the polymer lobes increasing slightly with power. Remarkably, the polymer is confined in two lobes and no trace of polymer is detected between the two lobes, suggesting an induced reaction with strong spatial control.

Figure 3e shows the results obtained for the two different polarization directions, i.e. the one along the triangle edge (corresponding to the Y polarization in simulated maps) and the one along the median of the triangles (corresponding to the X polarization in simulated maps) The results are highly reproducible for all the NPs observed (four particles for each irradiation), with polymer localization on one or two apexes respectively, depending on the polarization direction.

These results obtained with F_{DIAMS} (143°C), are compared with PETA (216°C), the monomer without the thermal initiator. It should be recalled that this system also shows no absorption at 800 nm The results are shown in **Figure 4**.

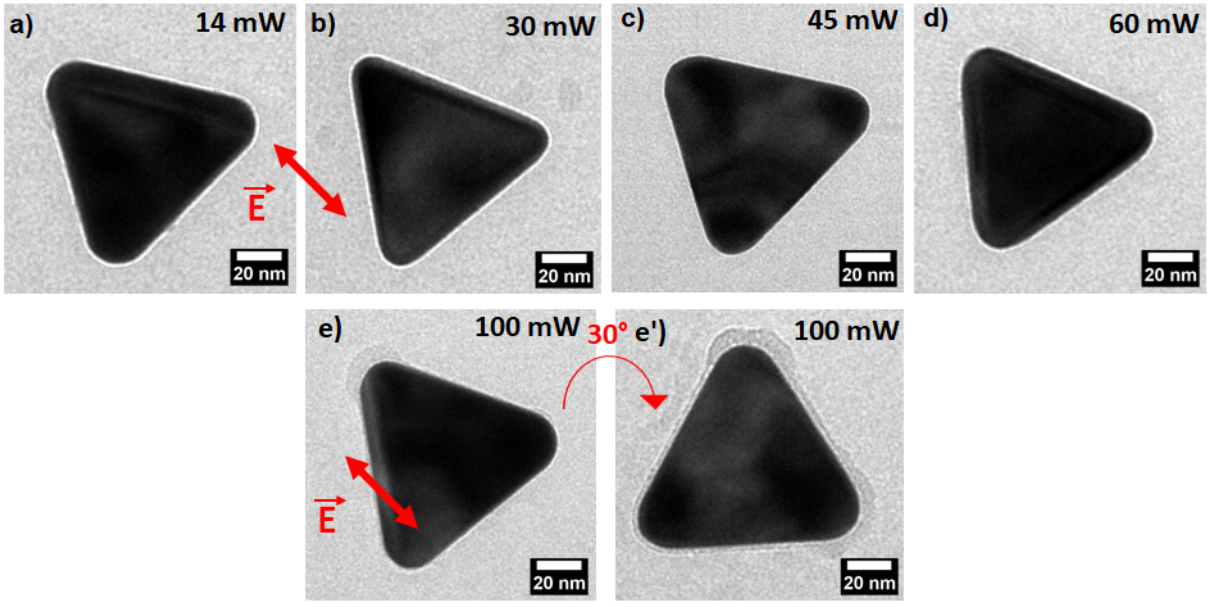

Figure 4. TEM images of AuNPs after irradiation in F_{PETA} at different powers: **a**) 14 mW, **b**) 30 mW, **c**) 45 mW, **d**) 60 mW. **e**) 100 mW. **e'**) Effect of polarization direction on polymerization of PETA at 100mW (direction of polarization is given by the red arrow).

No polymer was observed at the lowest power levels, including those that led to polymerization in the case of FDIAMS (30 - 60 mW). This demonstrates the decisive role of DIAMS in the polymerization mechanism. At 100 mW, polymer is observed on one of the apexes. As before,

the polymer is located on the apex in the direction of polarization of the incident light. At such power, we also observe that the position of the polymer lobes follows the direction of polarization (Figure 4b). In this case, a thin polymer layer is also observed, demonstrating the poorer spatial confinement of the reaction for such conditions.

These results with F_{DIAMS} clearly demonstrate the possibility of inducing a confined anisotropic polymerization reaction on the surface of nanoparticles. We should now answer the question of the origin of this polymerization reaction, given that the resins were originally designed to react according to a thermally-induced radical polymerization mechanism.

It should be remembered that in the absence of nanoparticles, no reaction is observed, even at much higher powers, which clearly indicates a role for nanoparticles in the mechanism and the elimination of a purely photochemical mechanism (there is no absorption of the formulation at 800 nm).

On the other hand, a mechanism involving hot charge carriers (electrons or holes) could explain the observed reaction, especially as this phenomenon is favored in the pulsed regime and for nanostructures with angular corners. However, we have excluded this mechanism for the following reasons:

A reaction involving the transfer of hot carriers presupposes proximity between the chemical species accepting these hot carriers and the nanoparticles. In the case of F_{DIAMS}, the thermal initiator, which is clearly at the origin of polymerization, is not attached to the nanoparticle surface but diluted in the PETA, which can be considered a dielectric medium. Thus, the probability of polymerization initiation by this mechanism is highly improbable under these dilution conditions. On the other hand, part of the DIAMS molecules is used to locally consume the inhibitor of the radical reaction (oxygen).

Furthermore, in another study, Guselnikova et al functionalized their AuNPs with alkoxyamines close to DIAMS[55], thereby setting up conditions that theoretically favor the transfer of hot electrons by creating new electronic states between the adsorbate and the ANPs[56]. Despite this, Guselnikova et al conclude that no charged species are present by electron spin resonance (ESR) characterization, thus ruling out direct hot carriers transfer in their study[55].

Furthermore, in a recent study, the same formulation (F_{DIAMS}) was used to demonstrate thermoplasmonic polymerization on a scale of several tens of microns[42]. The heat required to induce polymerization of F_{DIAMS} is clearly initiated by the thermoplasmonic effect induced by

the dense network of AuNPs. The polymerized thickness of several tens of microns eliminates the hypothesis of initiation by the transfer of hot electrons throughout the polymerized volume, given that the polymer has no electronic conduction properties[57]. This study confirms the possibility of initiating thermal polymerization by the thermoplasmonic effect, even though these experiments were carried out under continuous irradiation, unlike the present work, which was carried out under femtosecond pulsed irradiation.

The electronic properties of the thermopolymerizable resin used in this study are therefore very different from those of materials previously used in a similar context for charge transfer polymerization. Concerning the work of Nguyen et al[58,59] for example, before depositing the polymerizable formulation, they functionalize their NPs by electrochemical grafting with thin layers of diazonium salts (known to be good hot electron acceptors).[58,59]After functionalization, they irradiate their NPs in the presence of a monomer to trigger near-field polymerization. In this case, charge transfer is made possible by chemical grafting to the surface of the NPs and also by the redox properties of the molecular systems. These conditions are not met in our case, and polymerization reaction is observed in two different systems (F_{DIAMS} and PETA).

Finally, these observations allow us to conclude on the thermal nature of the polymerization reaction. Considering the thermal polymerization thresholds of the FDIAMS and PETA formulations, we can conclude that the respective polymerization temperatures (143°C and 216°C) are reached at the nanoparticle surface. But beyond this interesting result, the remarkable finding is the observation of polymer lobes of nanometric size and localized on particular points of the nanoparticle corresponding to the maximum field regions. In other words, this result shows that heat exchange between the triangular nanoparticle and the surrounding medium is highly anisotropic. These results therefore contradict the usual description of temperature homogenization in the nanoparticle being too fast for heat exchange with the external environment to be localized to parts of the nanoparticle. This method of characterizing temperature on a local scale by chemical processes thus provides, for the first time, a snapshot of the temperature distribution around the nanoparticle. In particular, it challenges the view that heat exchange in the nanoparticle is exclusively isotropic after thermal relaxation.

These results should be considered in comparison with the simple physical models of thermal diffusion usually used to describe heat diffusion in a spherical metal particle and from the particle to the surrounding medium.

For example, the characteristic thermal diffusion time in a spherical metal nanoparticle of the same volume as the nanotriangle used here can be estimated using the classic Fick diffusion formula [60] :

$$\tau_d^{Au} = \frac{R^2}{4D_{Au}}$$

Taking R = 20 nm and D_{Au} = 1.2 x10^{-4} m^2/s, we calculate τ_d^{Au}=850 fs. As expected, the time determined in this model is very short compared with the time required to diffuse this thermal energy from a nanoparticle of the same volume to the external environment, which can be evaluated using the following formula [61] :

$$\tau_d^s = \frac{\rho_{Au} C_{Au} R^2}{3K_s}$$

where ρ_{Au} is the mass density of the AuNP (19.32 ×10^3 kg/m^3) and C_{Au} its specific heat capacity at constant pressure (129 J/kg/K). K_s is the mean thermal conductivity[61] of the surrounding medium and substrate (K_{PMMA} = 0.19 W/m/K and K_{SI3N4} = 22 W/m/K).

It is found τ_d^s =30 ps >> τ_d^{Au} . Assuming that the orders of magnitude remain the same for the nanoparticles used in our study, we can see that these models fail to account for non-isotropic heat diffusion around nanoparticles.

Classical models therefore suggest that heat transfer is homogeneous and isotropic around the NP. Observation of localized lobes obtained by thermal polymerization tells us that heat transfer to the thermally polymerizable resin is ultimately very rapid, preventing complete homogenization of the NP's temperature.

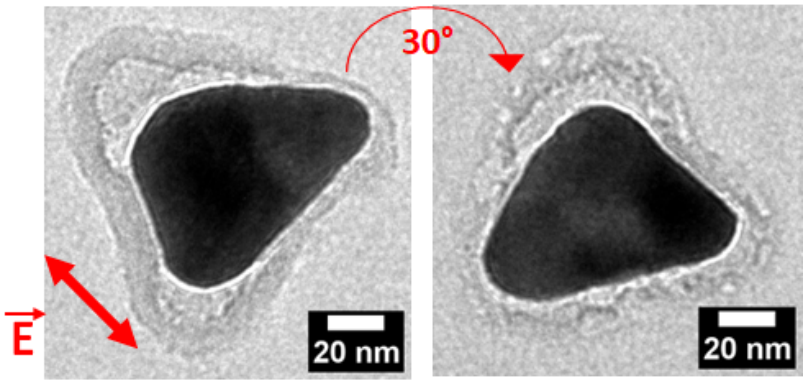

Figure 5. Anisotropic change of NPs shape at high power under different polarization states. (200 mW).

These results are also confirmed by observations made at high powers. Figure 5 indeed shows the morphological modifications observed in the nanoobjects for powers of 200 mW, under different polarization directions. As expected, polymerization took place, as evidenced by the gray crown visible on the TEM image. We find a main contribution in the direction of polarization, in agreement with the results at lower power. In this case we also observe a homogeneous layer all around the NP, meaning that the polymerization temperature has been reached over the entire periphery of the NP.

It is also evident that the nanoparticles have been modified under these power conditions. By comparing to the direction of polarization, we see that the affected apexe(s) are those located in the direction of polarization. The trace of the polymer corresponds to the section of the nanoparticle before reconfiguration, which also allows us to conclude that the polymerization took place on a faster time scale than that of the reconfiguration of the nanoparticle.

Such restructuring of nanoparticles under laser irradiation have already been observed by Viarbitskaya et al[17] and Zhang et al[15]. These results are in agreement with various simulation works showing that the electronic temperature is non-homogeneous following irradiation in pulsed regime. They thus allow us to confirm temperature exchange at the nanometric scale.

Conclusion

We have shown in this study that it is possible to generate extremely localized nanosources of heat by excitation of the plasmon resonance of gold nanotriangles. This result is obtained for thermopolymerizable formulations which show no absorbance at the wavelength considered (800 nm). These polymer lobes appear in the maximum field region, which depend on the polarization of the incident light.

This study therefore converges towards the existence of a transient regime in which a strong temperature gradient is present at the nanoparticle level. Our study shows for the first time experimentally that it is possible to transfer this heat to a material directly in contact with the surface of the nanoparticle before thermal homogenization. The thermopolymer used in this study thus has a response fast enough for the reaction to be triggered before the temperature is uniform at the nanoparticle level. The exact process of this energy transfer, however, remains to be elucidated in detail. In particular, different thermally polymerizable systems could be considered to elucidate this mechanism.

Acknowledgments

The authors want to thank Gauthier Schrodj (IS2M) for carrying out the DSC measurement, Loic Vidal (IS2M) for imaging the AuNTs with TEM, and Yohann Guillaneuf (ICR, Marseille) for providing the thermal iniator DIAMS. The authors acknowledge ANR for funding (POPCORN grant numbers ANR-21-CE09-0035). This work of the Interdisciplinary Institute HiFunMat, as part of the ITI 2021–2028 program of the University of Strasbourg, CNRS and Inserm, was supported by IdEx Unistra (ANR-10-IDEX-0002) and SFRI (STRAT'US project, ANR-20-SFRI-0012) under the framework of the French Investments for the Future Program.

TOC

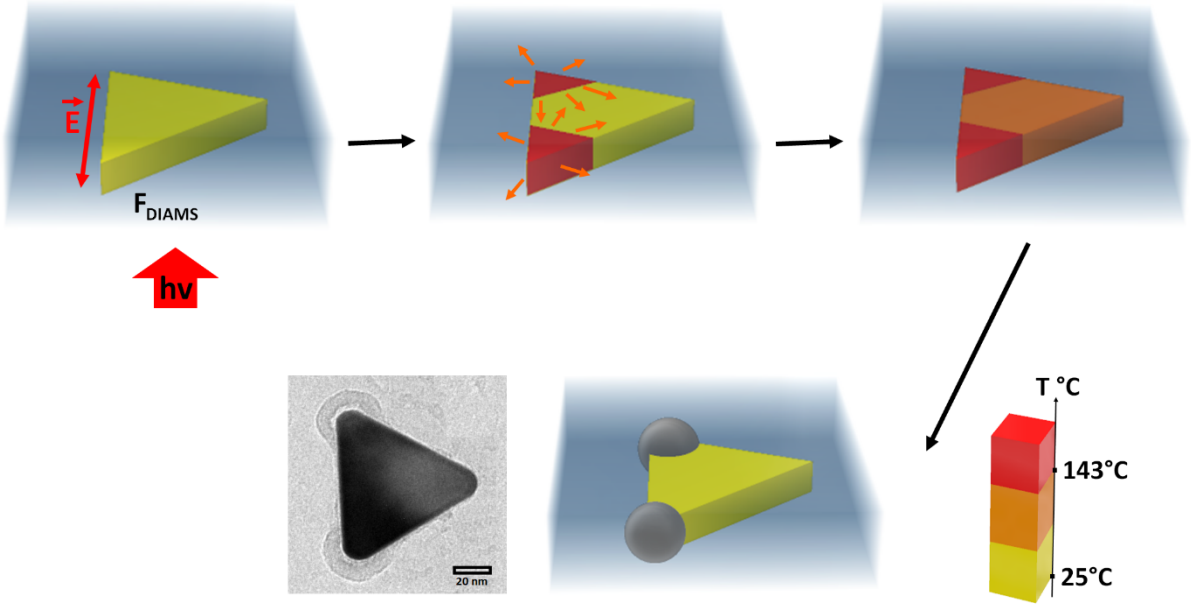

References

(1) Porcel, E.; Liehn, S.; Remita, H.; Usami, N.; Kobayashi, K.; Furusawa, Y.; Le Sech, C.; Lacombe, S. Platinum Nanoparticles: A Promising Material for Future Cancer Therapy? *Nanotechnology* **2010**, *21* (8), 085103.

(2) Ma, N.; Jiang, Y.-W.; Zhang, X.; Wu, H.; Myers, J. N.; Liu, P.; Jin, H.; Gu, N.; He, N.; Wu, F.-G.; Chen, Z. Enhanced Radiosensitization of Gold Nanospikes via Hyperthermia in Combined Cancer Radiation and Photothermal Therapy. *ACS Appl. Mater. Interfaces* **2016**, *8* (42), 28480–28494. https://doi.org/10.1021/acsami.6b10132.

(3) Khitous, A.; Noel, L.; Molinaro, C.; Vidal, L.; Grée, S.; Soppera, O. Sol–Gel TiO2 Thin Film on Au Nanoparticles for Heterogeneous Plasmonic Photocatalysis. *ACS Appl. Mater. Interfaces* **2024**. https://doi.org/10.1021/acsami.3c15866.

(4) Brissaud, C.; Besteiro, L. V.; Piquemal, J.-Y.; Comesaña-Hermo, M. Plasmonics: A Versatile Toolbox for Heterogeneous Photocatalysis. *Solar RRL* **2023**.

(5) Li, J.; Cushing, S. K.; Meng, F.; Senty, T. R.; Bristow, A. D.; Wu, N. Plasmon-Induced Resonance Energy Transfer for Solar Energy Conversion. *Nature Photonics* **2015**, *9* (9), 601–607.

(6) Li, Y.; Verbiest, T.; Vankelecom, I. Improving the Flux of PDMS Membranes via Localized Heating through Incorporation of Gold Nanoparticles. *Journal of membrane science* **2013**, *428*, 63–69.
(7) Lin, C.-F.; Khitous, A.; Zan, H.-W.; Soppera, O. Exploiting Thermoplasmonic Effects for Laser-Assisted Preparation of Au Nanoparticles/InZnO Thin Film with Visible Range Photodetection Properties. *Advanced Optical Materials* **2021**, *9* (22), 2100045.
(8) Noel, L.; Khitous, A.; Molinaro, C.; Zan, H.; Berling, D.; Grasset, F.; Soppera, O. Laser Direct Writing of Crystallized TiO_2 by Photothermal Effect Induced by Gold Nanoparticles. *Adv Materials Technologies* **2023**, 2300407. https://doi.org/10.1002/admt.202300407.
(9) Pop, E. Energy Dissipation and Transport in Nanoscale Devices. *Nano Res.* **2010**, *3* (3), 147–169. https://doi.org/10.1007/s12274-010-1019-z.
(10) Li, N.; Ren, J.; Wang, L.; Zhang, G.; Hänggi, P.; Li, B. Phononics: Manipulating Heat Flow with Electronic Analogs and Beyond. *Rev. Mod. Phys.* **2012**, *84* (3), 1045–1066. https://doi.org/10.1103/RevModPhys.84.1045.
(11) Cui, L.; Miao, R.; Jiang, C.; Meyhofer, E.; Reddy, P. Perspective: Thermal and Thermoelectric Transport in Molecular Junctions. *The Journal of Chemical Physics* **2017**, *146* (9).
(12) Nitzan, A.; Ratner, M. A. Electron Transport in Molecular Wire Junctions. *Science* **2003**, *300* (5624), 1384–1389. https://doi.org/10.1126/science.1081572.
(13) Nearingburg, B.; Elias, A. L. Characterization of Surface Plasmon Energy Transduction in Gold Nanoparticle/Polymer Composites by Photo-DSC. *Thermochimica acta* **2011**, *512* (1–2), 247–253.
(14) Richardson, H. H.; Carlson, M. T.; Tandler, P. J.; Hernandez, P.; Govorov, A. O. Experimental and Theoretical Studies of Light-to-Heat Conversion and Collective Heating Effects in Metal Nanoparticle Solutions. *Nano Lett.* **2009**, *9* (3), 1139–1146. https://doi.org/10.1021/nl8036905.
(15) Zhang, Y.; Shi, L.; Hu, D.; Chen, S.; Xie, S.; Lu, Y.; Cao, Y.; Zhu, Z.; Jin, L.; Guan, B.-O. Full-Visible Multifunctional Aluminium Metasurfaces by in Situ Anisotropic Thermoplasmonic Laser Printing. *Nanoscale Horizons* **2019**, *4* (3), 601–609.
(16) Wang, D.; Koh, Y. R.; Kudyshev, Z. A.; Maize, K.; Kildishev, A. V.; Boltasseva, A.; Shalaev, V. M.; Shakouri, A. Spatial and Temporal Nanoscale Plasmonic Heating Quantified by Thermoreflectance. *Nano Lett.* **2019**, *19* (6), 3796–3803. https://doi.org/10.1021/acs.nanolett.9b00940.
(17) Viarbitskaya, S.; Cuche, A.; Teulle, A.; Sharma, J.; Girard, C.; Arbouet, A.; Dujardin, E. Plasmonic Hot Printing in Gold Nanoprisms. *ACS photonics* **2015**, *2* (6), 744–751.
(18) Baffou, G. Anti-Stokes Thermometry in Nanoplasmonics. *ACS Nano* **2021**, *15* (4), 5785–5792. https://doi.org/10.1021/acsnano.1c01112.
(19) Baffou, G. Thermoplasmonics: Heating Metal Nanoparticles Using Light; 2017.
(20) Kim, K.; Jeong, W.; Lee, W.; Reddy, P. Ultra-High Vacuum Scanning Thermal Microscopy for Nanometer Resolution Quantitative Thermometry. *ACS Nano* **2012**, *6* (5), 4248–4257. https://doi.org/10.1021/nn300774n.
(21) Coppens, Z. J.; Li, W.; Walker, D. G.; Valentine, J. G. Probing and Controlling Photothermal Heat Generation in Plasmonic Nanostructures. *Nano Lett.* **2013**, *13* (3), 1023–1028. https://doi.org/10.1021/nl304208s.
(22) Carrillo-Torres, R. C.; García-Soto, M. J.; Morales-Chávez, S. D.; Garibay-Escobar, A.; Hernández-Paredes, J.; Guzmán, R.; Barboza-Flores, M.; Álvarez-Ramos, M. E. Hollow Au–

Ag Bimetallic Nanoparticles with High Photothermal Stability. *RSC advances* **2016**, *6* (47), 41304–41312.
(23) Pattani, V. P.; Tunnell, J. W. Nanoparticle-mediated Photothermal Therapy: A Comparative Study of Heating for Different Particle Types. *Lasers Surg Med* **2012**, *44* (8), 675–684. https://doi.org/10.1002/lsm.22072.
(24) Wang, Y.; Black, K. C. L.; Luehmann, H.; Li, W.; Zhang, Y.; Cai, X.; Wan, D.; Liu, S.-Y.; Li, M.; Kim, P.; Li, Z.-Y.; Wang, L. V.; Liu, Y.; Xia, Y. Comparison Study of Gold Nanohexapods, Nanorods, and Nanocages for Photothermal Cancer Treatment. *ACS Nano* **2013**, *7* (3), 2068–2077. https://doi.org/10.1021/nn304332s.
(25) Zhou, J.; Del Rosal, B.; Jaque, D.; Uchiyama, S.; Jin, D. Advances and Challenges for Fluorescence Nanothermometry. *Nature methods* **2020**, *17* (10), 967–980.
(26) Ngo, D. N.; Ho, V. T. T. X.; Kim, G.; Song, M. S.; Kim, M. R.; Choo, J.; Joo, S.-W.; Lee, S. Y. Raman Thermometry Nanopipettes in Cancer Photothermal Therapy. *Anal. Chem.* **2022**, *94* (17), 6463–6472. https://doi.org/10.1021/acs.analchem.1c04452.
(27) Molinaro, C.; Khitous, A.; Noel, L.; Soppera, O. Nanochemistry by Thermoplasmonic Effects. In *Progress in Nanophotonics 7*; Springer, 2022; pp 71–91.
(28) Besbes, M. SimPhotonics_FMM. **2023**.
(29) Bryche, J.-F.; Vega, M.; Moreau, J.; Karsenti, P.-L.; Bresson, P.; Besbes, M.; Gogol, P.; Morris, D.; Charette, P. G.; Canva, M. Ultrafast Heat Transfer at the Nanoscale: Controlling Heat Anisotropy. *ACS photonics* **2023**, *10* (4), 1177–1186.
(30) Khosravi Khorashad, L.; Besteiro, L. V.; Wang, Z.; Valentine, J.; Govorov, A. O. Localization of Excess Temperature Using Plasmonic Hot Spots in Metal Nanostructures: Combining Nano-Optical Antennas with the Fano Effect. *J. Phys. Chem. C* **2016**, *120* (24), 13215–13226. https://doi.org/10.1021/acs.jpcc.6b03644.
(31) Govorov, A. O.; Zhang, W.; Skeini, T.; Richardson, H.; Lee, J.; Kotov, N. A. Gold Nanoparticle Ensembles as Heaters and Actuators: Melting and Collective Plasmon Resonances. *Nanoscale Research Letters* **2006**, *1*, 84–90.
(32) Govorov, A. O.; Richardson, H. H. Generating Heat with Metal Nanoparticles. *Nano today* **2007**, *2* (1), 30–38.
(33) Cheng, Z.; Liu, L.; Xu, S.; Lu, M.; Wang, X. Temperature Dependence of Electrical and Thermal Conduction in Single Silver Nanowire. *Scientific reports* **2015**, *5* (1), 10718.
(34) Lin, H.; Xu, S.; Li, C.; Dong, H.; Wang, X. Thermal and Electrical Conduction in 6.4 Nm Thin Gold Films. *Nanoscale* **2013**, *5* (11), 4652–4656.
(35) Anderson, J. H. Measurement of Thermal Conductivity of Gold Nanofilms and Nanowires. PhD Thesis, Texas State University, 2020.
(36) Taylor, A. B.; Siddiquee, A. M.; Chon, J. W. M. Below Melting Point Photothermal Reshaping of Single Gold Nanorods Driven by Surface Diffusion. *ACS Nano* **2014**, *8* (12), 12071–12079. https://doi.org/10.1021/nn5055283.
(37) khitous, A. Spatial Distribution of the Photopolymerization Induced by Localized Surface Plasmons: Impact of the Morphology of the Au Nanoparticles.
(38) Kameche, F.; Heni, W.; Telitel, S.; Vidal, L.; Marguet, S.; Douillard, L.; Fiorini-Debuisschert, C.; Bachelot, R.; Soppera, O. Probing Plasmon-Induced Chemical Mechanisms by Free-Radical Nanophotopolymerization. *The Journal of Physical Chemistry C* **2021**, *125* (16), 8719–8731.
(39) Kameche, F.; Heni, W.; Telitel, S.; Ge, D.; Vidal, L.; Dumur, F.; Gigmes, D.; Lalevee, J.; Marguet, S.; Douillard, L. Plasmon-Triggered Living Photopolymerization for Elaboration of Hybrid Polymer/Metal Nanoparticles. *Materials Today* **2020**, *40*, 38–47.

(40) Deeb, C.; Ecoffet, C.; Bachelot, R.; Plain, J.; Bouhelier, A.; Soppera, O. Plasmon-Based Free-Radical Photopolymerization: Effect of Diffusion on Nanolithography Processes. *Journal of the American Chemical Society* **2011**, *133* (27), 10535–10542.
(41) Khitous, A.; Lartigue, L.; Moreau, J.; Soppera, O. Insights into Photopolymerization at the Nanoscale Using Surface Plasmon Resonance Imaging. *Small n/a* (n/a), 2401885. https://doi.org/10.1002/smll.202401885.
(42) Molinaro, C.; Khitous, A.; Soppera, O. Chemical Method Based on Thermally Activated Free Radical Polymerization to Determine the Temperature in Thermoplasmonics. *ACS Appl. Polym. Mater.* **2024**, *6* (9), 5331–5338. https://doi.org/10.1021/acsapm.4c00525.
(43) Mitiche, S.; Marguet, S.; Charra, F.; Douillard, L. Plasmonics of Regular Shape Particles, a Simple Group Theory Approach. *Nano Res.* **2020**, *13* (6), 1597–1603. https://doi.org/10.1007/s12274-020-2776-y.
(44) Khitous, A.; Molinaro, C.; Abdellah, S.; Marguet, S.; Laurent, G.; Vidal, L.; Malval, J.-P.; Fiorini-Debuisschert5, C.; Adam, P.-M.; Douillard, L.; Bachelot, R.; Soppera, O. Spatial Distribution of the Photopolymerization Induced by Localized Surface Plasmons: Impact of the Morphology of the Au Nanoparticles. *The Journal of Physical Chemistry C*. 2024.
(45) Charleux, B.; Nicolas, J. Water-Soluble SG1-Based Alkoxyamines: A Breakthrough in Controlled/Living Free-Radical Polymerization in Aqueous Dispersed Media. *Polymer* **2007**, *48* (20), 5813–5833.
(46) Nicolas, J.; Ruzette, A.-V.; Farcet, C.; Gérard, P.; Magnet, S.; Charleux, B. Nanostructured Latex Particles Synthesized by Nitroxide-Mediated Controlled/Living Free-Radical Polymerization in Emulsion. *Polymer* **2007**, *48* (24), 7029–7040.
(47) Hohenester, U.; Trügler, A. MNPBEM–A Matlab Toolbox for the Simulation of Plasmonic Nanoparticles. *Computer Physics Communications* **2012**, *183* (2), 370–381.
(48) Waxenegger, J.; Trügler, A.; Hohenester, U. Plasmonics Simulations with the MNPBEM Toolbox: Consideration of Substrates and Layer Structures. *Computer Physics Communications* **2015**, *193*, 138–150.
(49) Luke, K.; Okawachi, Y.; Lamont, M. R.; Gaeta, A. L.; Lipson, M. Broadband Mid-Infrared Frequency Comb Generation in a Si 3 N 4 Microresonator. *Optics letters* **2015**, *40* (21), 4823–4826.
(50) Johnson, P. B.; Christy, R. W. Optical Constants of the Noble Metals. *Phys. Rev. B* **1972**, *6* (12), 4370–4379. https://doi.org/10.1103/PhysRevB.6.4370.
(51) Khitous, A.; Molinaro, C.; Gree, S.; Haupt, K.; Soppera, O. Plasmon-Induced Photopolymerization of Molecularly Imprinted Polymers for Nanosensor Applications. *Advanced Materials Interfaces* **2023**, 2201651.
(52) Ge, D.; Issa, A.; Jradi, S.; Couteau, C.; Marguet, S.; Bachelot, R. Advanced Hybrid Plasmonic Nano-Emitters Using Smart Photopolymer. *Photonics research* **2022**, *10* (7), 1552–1566.
(53) Kou, X.; Ni, W.; Tsung, C.-K.; Chan, K.; Lin, H.-Q.; Stucky, G. D.; Wang, J. Growth of Gold Bipyramids with Improved Yield and Their Curvature-Directed Oxidation. *Small* **2007**, *3* (12), 2103–2113.
(54) Aoudjit, T.; Horrer, A.; Kostcheev, S.; Bachelot, R.; Plain, J.; Gérard, D. Photochemical Imaging of Near-Field and Dissymmetry Factor in Chiral Nanostructures. *Advanced Optical Materials* **2023**, *11* (9), 2203015.
(55) Guselnikova, O.; Audran, G.; Joly, J.-P.; Trelin, A.; Tretyakov, E. V.; Svorcik, V.; Lyutakov, O.; Marque, S. R.; Postnikov, P. Establishing Plasmon Contribution to Chemical Reactions: Alkoxyamines as a Thermal Probe. *Chemical science* **2021**, *12* (11), 4154–4161.

(56) Boerigter, C.; Aslam, U.; Linic, S. Mechanism of Charge Transfer from Plasmonic Nanostructures to Chemically Attached Materials. *ACS nano* **2016**, *10* (6), 6108–6115.
(57) Blandre, E.; Jalas, D.; Petrov, A. Yu.; Eich, M. Limit of Efficiency of Generation of Hot Electrons in Metals and Their Injection inside a Semiconductor Using a Semiclassical Approach. *ACS Photonics* **2018**, *5* (9), 3613–3620. https://doi.org/10.1021/acsphotonics.8b00473.
(58) Nguyen, M.; Lamouri, A.; Salameh, C.; Lévi, G.; Grand, J.; Boubekeur-Lecaque, L.; Mangeney, C.; Félidj, N. Plasmon-Mediated Chemical Surface Functionalization at the Nanoscale. *Nanoscale* **2016**, *8* (16), 8633–8640.
(59) Nguyen, V.-Q.; Ai, Y.; Martin, P.; Lacroix, J.-C. Plasmon-Induced Nanolocalized Reduction of Diazonium Salts. *ACS Omega* **2017**, *2* (5), 1947–1955. https://doi.org/10.1021/acsomega.7b00394.
(60) Baffou, G.; Rigneault, H. Femtosecond-Pulsed Optical Heating of Gold Nanoparticles. *Physical Review B* **2011**, *84* (3), 035415.
(61) Baffou, G.; Berto, P.; Bermúdez Ureña, E.; Quidant, R.; Monneret, S.; Polleux, J.; Rigneault, H. Photoinduced Heating of Nanoparticle Arrays. *Acs Nano* **2013**, *7* (8), 6478–6488.